



Article citation info:

Rosiński A, Paś J, Bialek K, Wetoszka P, Method for Assessing Reliability of the Power Supply System for Electronic Security Systems of Intelligent Buildings Taking Into Account External Natural Interference, *Eksploracja i Niezawodność – Maintenance and Reliability* 2024; 26(1) <http://doi.org/10.17531/ein/176375>

## Method for Assessing Reliability of the Power Supply System for Electronic Security Systems of Intelligent Buildings Taking Into Account External Natural Interference

Indexed by:



Adam Rosiński<sup>a,\*</sup>, Jacek Paś<sup>b</sup>, Kamil Bialek<sup>c</sup>, Patryk Wetoszka<sup>c</sup>

<sup>a</sup> Department of Air Transport Engineering and Teleinformatics, Faculty of Transport, Warsaw University of Technology, Poland

<sup>b</sup> Faculty of Electronic, Military University of Technology, Poland

<sup>c</sup> Signalling and Telecommunication Laboratory, Railway Research Institute, Poland

### Highlights

- The evaluation of impact of interference on power supply of electronic security systems can be difficult.
- Theoretical discussions have been confirmed by surge arrester measurements.
- A reliability analysis of electronic security system power supply was conducted.
- A method for assessing the power supply continuity in electronic security systems was developed.

### Abstract

The article presents issues related to the reliability of power supply for electronic security devices in intelligent buildings. These systems function under varied environmental conditions and are exposed to external or internal natural and artificial interference; lightning, in particular. The authors conducted actual experimental tests of two surge arresters that are used to protect against a lightning impulse. As a result of conducted tests, followed by reliability and operational modelling, it was concluded that their use in internal connection structures increased the probability of a system staying in a state of full fitness. All of the deliberations included in the article enabled developing a new method for assessing the power supply continuity in electronic security systems of intelligent buildings, taking into account external natural interference. This method can also be applied to assess the power supply continuity in other electronic systems and devices.

### Keywords

power supply continuity, electronic security systems, electromagnetic interference, surge arrester

This is an open access article under the CC BY license (<https://creativecommons.org/licenses/by/4.0/>)

### 1. Introduction

The development of technical systems for managing the I&C of buildings and electronic security systems (ESS) [1-3] (e.g., closed-circuit television (CCTV), fire alarm systems (FAS), audio warning systems (AWS), intrusion detection systems (IDS), access control systems (ACS), etc.) entails increasing miniaturization and “clustering” of elements in given modules within these technical structures [4]. Individual ESS functional components require less and less supply power for their correct functioning. Such a manner of protecting ESS systems during

a power failure requires smaller capacities of batteries treated as backup power sources (especially in rail transport, where the issue of ensuring passenger safety is vital [5-8]). ESS is supplied via a power line downstream a fire switch, while the FAS upstream of this device, due to the role of this system in ensuring building security (Fig. 1) [9,10]. The FAS power supply is always provided from before the fire switch, as shown in Fig. 1. This allows the entire security system to function even in the event of a fire. During the initial period of the fire, the

(\*) Corresponding author.

E-mail addresses:

A. Rosiński (ORCID: 0000-0002-1776-9540) [adam.rosinski@pw.edu.pl](mailto:adam.rosinski@pw.edu.pl), J. Paś (ORCID: 0000-0001-8900-1445) [jacek.pas@wat.edu.pl](mailto:jacek.pas@wat.edu.pl), K. Bialek (ORCID: 0000-0002-9982-1145) [kbialek@ikolej.pl](mailto:kbialek@ikolej.pl), P. Wetoszka (ORCID: 0000-0002-0329-7861) [pwetoszka@ikolej.pl](mailto:pwetoszka@ikolej.pl),

officer in charge of the fire extinguishing operation has the ability to view all the technical status of the elements and devices installed in the FAS on the FAC panel. The power supply in all FAS is provided by the FAC, where there is a dedicated power supply generating a voltage of  $\pm 24$  [V]. This voltage value is safe for all people involved in firefighting.

However, the application of such technical solutions in electronic building management systems leads to the amount of energy needed to disrupt or even damage individual elements or devices within these systems is decreasing. This is why, taking into account electromagnetic compatibility and determining the resistance, strength and susceptibility of individual elements and devices to conducted and radiated interference is an important issue, already at the ESS design stage [11-13]. The efficient operation of all technical systems in modern intelligent buildings is ensured by the following management systems:

- BMS (Building Management System) – system for

managing all technical functions of a building – including a power supply subsystem, electricity control and comfort – e.g., air-conditioning,

- SMS (Security Management System) – system for managing all electronic security systems of a building – CCTV [14], FAS [15,16], IDS, ACS, etc.,
- BMCS (Building Management and Control System) is a global building management and control system that integrates BMS and SMS. Its objective is collecting and analysing information from the entire facility (e.g., Alarm Receiving Centre (ARC), as well as the exchange of data between all cooperating subsystems [17,18],
- EMS (Energy Management System) – system for managing electricity [19,20] and thermal energy.

The use of integrated systems enables efficient management of the safety and user comfort associated with a given building.

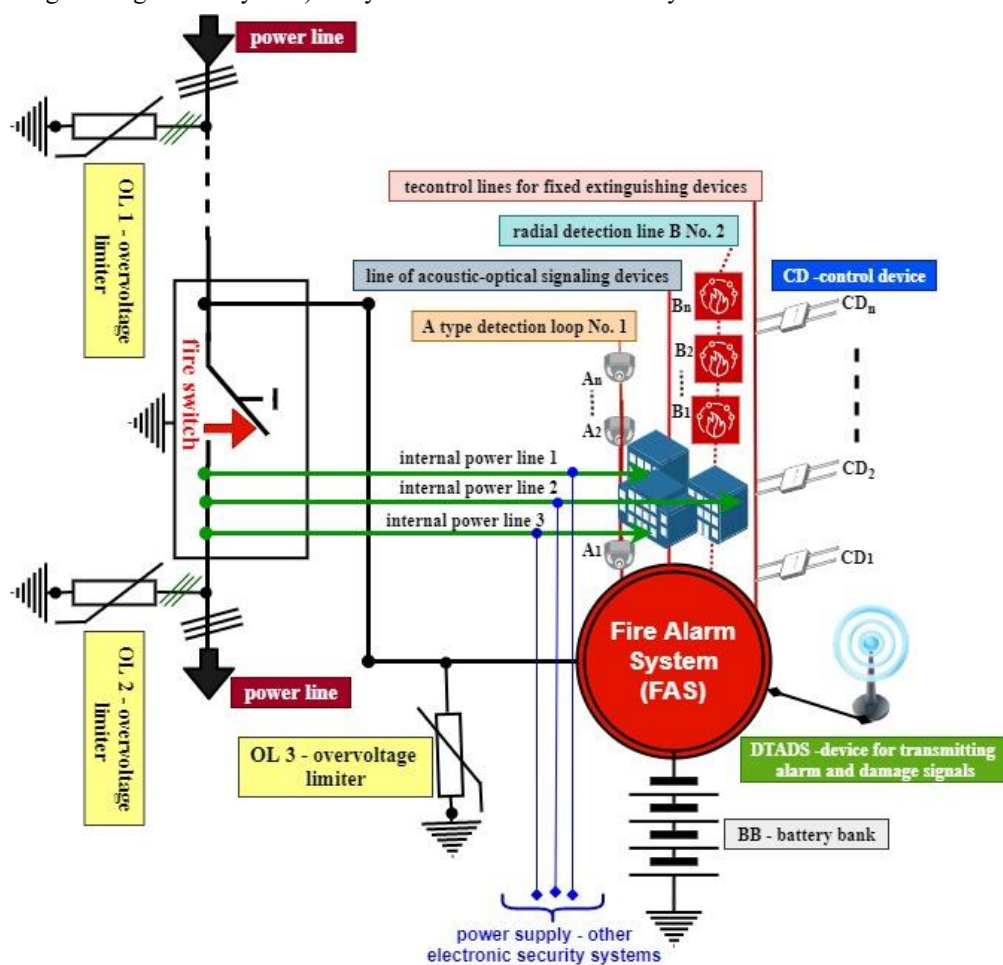


Fig. 1. Power supply for an ESS and fire alarm system (FAS).

Overvoltage occurring in power lines supplying electronic management systems inside intelligent building may be caused by [21-23]:

- power line switching activities – the so-called internal overvoltage propagating in HV (highest voltage), MV (medium voltage) and LV (low voltage) power lines,

associated with e.g., high inertia of control devices, deactivation of short-circuits through fuses or activation/deactivation of consumers – e.g., capacitor banks or unloaded high-power motors and transformers – oscillatory nature of the overvoltage, and the interference range from 50 [Hz] to several [kHz], the interference frequency band is a function of – capacity, device load nature – Fig. 2, 3 (overvoltage graphs are presented for four external transformer stations supplied with 30 [kV] from a power grid),

- lightning discharges – external overvoltage, with a random interference level (amplitude),
- internal overvoltage associated with the so-called static electricity, which has always accompanied humans – users of a given building in the era of using various artificial materials – e.g., PVC (polyvinyl chloride) carpets or flooring. Short-circuit isolators are used in detection loops of fire alarm systems (FAS). In this device, the supply

voltage is comparable to the reference voltage developed in this insulator. In the event of a short circuit, the supply voltage of all elements connected to the detection loop changes, e.g. detectors, modules, manual fire alarms, etc. Then, the electronic system of the short circuit isolator turns on the keying transistor. The detection loop is cut off on one side and power is supplied from the fire alarm control panel (FAC) on the other side. This gives us continuity of operation because only the section of the loop where the short circuit occurs is disabled. Short-circuit isolators are only used in FAS when using detection loops connected to the FAC, which is then the power source.

Peak overvoltage values for these three cases may be significantly higher than, e.g., permissible insulation strength of electronic devices or elements, e.g., in an SMS system. This is why it is necessary to use adequate protective devices – internal within a building or external, e.g., on power lines.

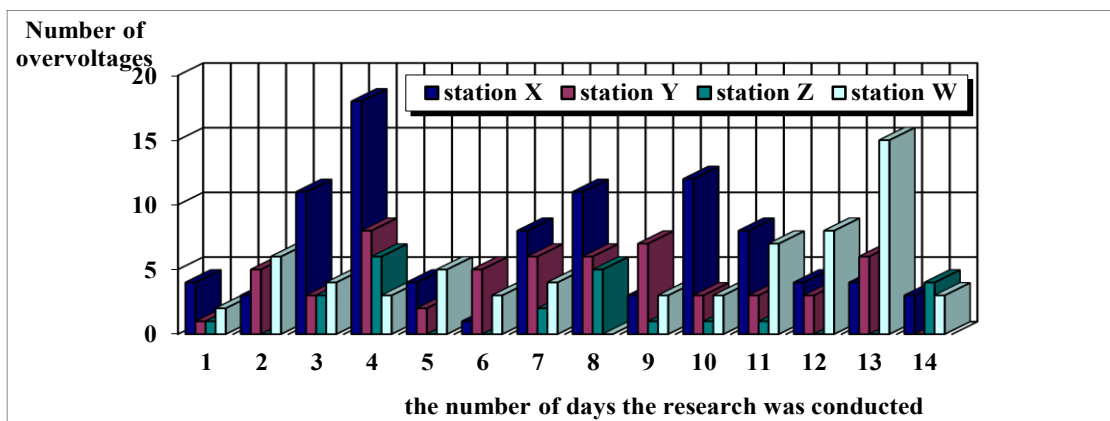


Fig. 2. Number of overvoltages n in building power supply systems. 230 V/50 [Hz] voltage, phase L1, 350-400 [V] overvoltages for four power stations X, Y, Z and W (own study – building ESS power supply at various switching stations).

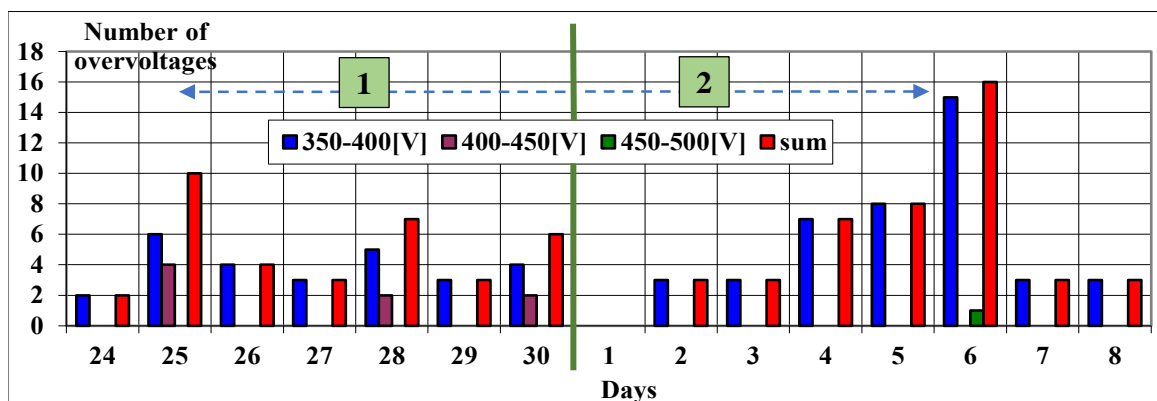


Fig. 3. Number of overvoltages in the 230 [V] / 50 [Hz] mains for phase L1, station W for individual days of the week (own study – building ESS power supply at various switching stations), legend: 1. max. disturbances in the power grid recorded in the first week of observation, 2. max. disturbances in the power grid recorded in the next week of observation.

So far, the publications known to the authors usually concentrated on overvoltage protections and their application in power grids. They include the work [24], the authors of which analysed normative and technical requirements regarding lightning protection systems. This stems from the fact that there is a need to apply additional protections against direct lightning strikes. They also compared overvoltage protection devices for low-voltage power grids. The conducted scientific deliberations enabled suggesting rational structural solutions and operational recommendations.

A large group of publications contains discussions on renewable energy sources (RES) and their cooperation with a power system [25-29]. Energy produced by wind and PV farms is transferred to distribution grids [30], while there can be adverse phenomena that reduce the reliability of a power system as a whole. This was presented in the study [31]. The basic source of energy for all electronic security systems is the generally available industrial power grid. In the event of damage to the above-mentioned power source, power is supplied from a battery bank, the capacity of which is determined separately for each case of use of these systems. In the case of using security systems in critical infrastructure facilities, an additional backup power source may be a generator or a UPS device. The conducted analysis enabled to draw a conclusion that current security systems utilize one group of settings that becomes ineffective with increasing level of distributed energy resource (DER) penetration. Therefore, the authors proposed the application of adaptive overcurrent protections.

Also [32] contains discussions on lightning and overvoltage protection both in large ground-based PV power plants, as well as small roof-mounted photovoltaic systems. It describes the fundamentals of lightning protection and the requirements for overvoltage protection. The author is right to state that despite so many solutions, there is still a need for the further introduction of modern solutions in this field. Also, the authors of [33] discussed the functioning of photovoltaic systems and suggested modifying the strategy of system switching.

A similar approach was presented in [34], where the authors elaborated on increasing system reliability by using active superconducting fault-current limiters (SFCL). The conducted simulation confirmed the justification behind applying such

solutions.

Protection systems were analysed in terms of reliability also in [35]. The article reviews the development of a power reliability scheme, which distinguishes between the power reliability characteristics of different DC protection diagrams.

An essential issue in the course of determining protections in power systems is designing protection systems adequately. Deliberations in this respect are included in [36]. The authors reviewed various optimization methodologies, which enables selecting proper solutions for coordinating protection devices.

Despite so many studies in the field of lightning and overvoltage protection solutions, there are no studies aimed directly at modelling and assessing the power supply continuity in electronic security systems of intelligent buildings, taking into account external high-altitude natural interference. This is why the authors of this article conducted tests in this regard.

## 2. The issue of protection against external overvoltages

External overvoltage caused by lightning are particularly dangerous due to the high peak amplitudes of interference signals up to 100 [kA] and more, short rise time (rise rate) up to 100 [kA/μs] and short duration  $t_i$  [37,38]. Lightning discharges close and directly into building lightning protection system rods can cause induction of high overvoltages in the receiving circuit loops of the power and ICT systems, buses or SMS system detection circuits, able to damage such equipment – Fig. 4.

The following values characterizing lightning current are required to evaluate the risk of lightning discharge damage in the case of electronic security systems:

- peak value –  $I_m$ ,
- maximum pulse rise rate  $S = \left(\frac{di_p}{dt}\right)_{max}$ ,
- load carried by surge current  $Q = \int i_p dt$ ,
- energy - pulse square pulse  $W = \int i_p^2 dt$  (energy dissipated per  $R = 1[\Omega]$ ).

In order to mathematically describe time waveforms  $I$  and successive ground lightning discharges, the equation described by the following relationship is used:

$$i(t) = k_i I_m [\exp(-\alpha t) - \exp(-\beta t)] \quad (1)$$

where:  $I_m$  – maximum current;  $k_i$  – correction factor,  $\alpha$ ,  $\beta$  – factors specifying leading edge duration and time to half-peak.

In such a case, the discharge current spectrum can be

expressed by the equation:

$$I(w) = k_I I_m \left( \frac{1}{\alpha + jw} - \frac{1}{\beta + jw} \right) = \frac{k_I I_m (\beta - \alpha)}{(\alpha + jw)(\beta + jw)} \quad (2)$$

The source literature contains numerous relationships describing discharge current waveforms constructed based on Heidler's formula – expression:

$$i(t) = \frac{I_m}{\eta} \frac{(t/\tau_1)^N}{1 + (t/\tau_1)^N} \exp(-t/\tau_2) \quad (3)$$

where:  $2 \leq N \leq 10$ , whereas the correction factor  $\eta$  is determined by the relationship:

$$\eta = \exp\left[-\left(\frac{\tau_1}{\tau_2}\right)\left(N \frac{\tau_2}{\tau_1}\right)^{\frac{1}{N}}\right] \quad (4)$$

Tab. 1. Values of factors found in the equation describing ground discharge current.

Parameter	Symbol	Unit	200 [kA], 10/350 [ $\mu$ s]			
IEC model for ground discharge current - formulas (3, 4)						
Correction factor	$\eta$	-	0.93	0.986	0.993	0.903
Decay time factor	$\tau_1$	$\mu$ s	19	1.82	0.454	3.867
Decay time factor	$\tau_2$	$\mu$ s	485	285	143	66.507
Max. value moment	$t_{peak}$	$\mu$ s	31.44	3.57	0.95	6.1687

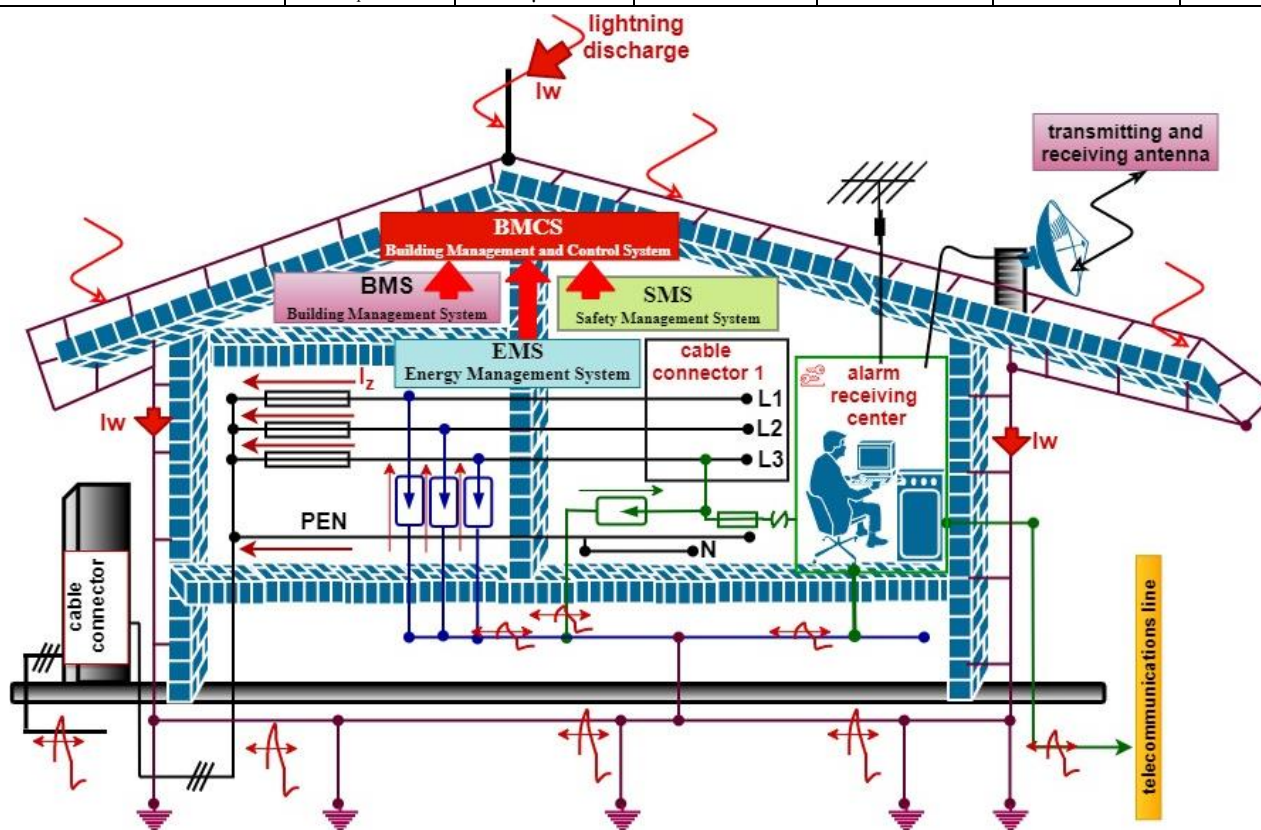


Fig. 4. Lightning discharges close and direct into the rods of the building lightning protection system, where:  $I_w$  – lightning discharge current value.

The overvoltage pulse value in electronic security systems depends on the environment surrounding the system devices – inside or outside of a protected facility. In order to evaluate the environment to which elements are ESS elements and devices are exposed, its following properties should be taken into account:

- factors associated with the area – facility with installed ESS,

- ESS exposure to the impact of lightning discharges – external or internal system elements and devices – cameras, sensors, perimeter building security, circuits, loops, or buses located within the building [39,40],
- technical and environmental conditions pertaining inside or outside of a given building due to existing solutions: earth electrodes, screening, ICT and teletechnical systems receiving circuit loops, ESS detection circuits or loops,

foundation earthing electrode execution, including the mutual inductance of magnetically coupled circuits  $M$  which determines overvoltage  $U_p$  induced in circuit loops –  $U_p = M \frac{di_w}{dt}$ , where:  $U_p$  – value of the overvoltage induced by a lightning discharge,  $di_w$  – lightning discharge current (Fig. 4),  $M$  – value of mutual inductance of magnetically coupled circuits within a building, e.g. earth electrode – detection circuit, earth electrode – power supply circuits, L1, L2, L3 supply circuits – detection circuits, etc.

In the course of conducting a spectral analysis of a lightning discharge pulse waveform, it can be concluded that the band up to several dozen [kHz] accumulates most energy of the primary discharge:

- approximately 80% of the total pulse energy is contained below 1 [kHz],
- approximately 99.5% of the total energy pulse energy is contained in the band up to 10 [kHz],
- approximately 99.6% of the total primary channel discharge energy is contained in the band up to 100 [kHz] – Fig. 5.

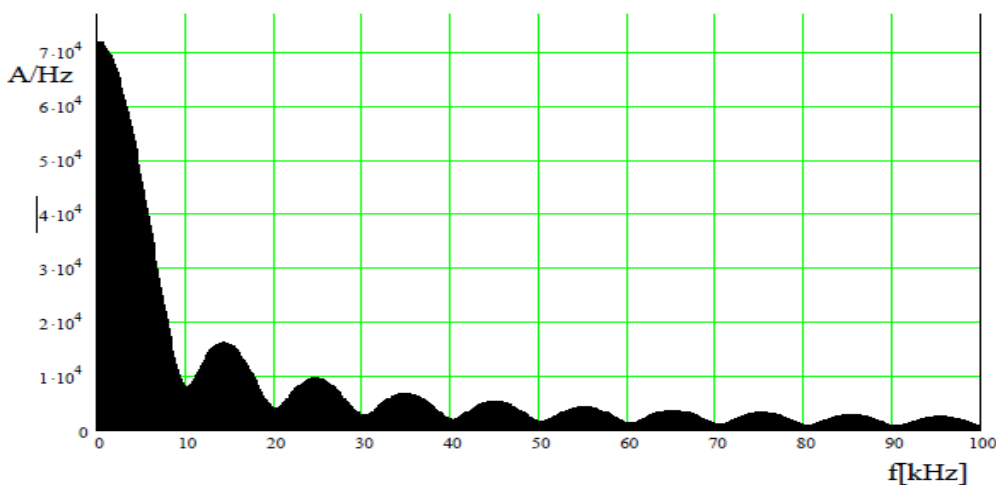


Fig. 5. Lightning discharge spectrum for a 100 [kA], 1/200 [μs] waveform.

Lightning discharge pulse for conducting a spectral analysis was described by the waveform according to Heidler’s formula:

$$i(t) = \frac{I_m}{\eta} \frac{(t/\tau_1)^N \exp(-t/\tau_2)}{1 + (t/\tau_1)^N} = \frac{I_m}{\exp\left[-\left(\frac{\tau_1}{\tau_2}\right) \left(N \frac{\tau_2}{\tau_1}\right)^{\frac{1}{N}}\right]} \frac{(t/\tau_1)^N \exp(-t/\tau_2)}{1 + (t/\tau_1)^N} \quad (5)$$

The following primary discharge current parameters were adopted to calculate the lightning discharge pulse spectrum, as per the model developed by IEC (for  $N = 10$ ):  $I_{w_{max}} = 100$  [kA], pulse leading edge time  $t_n = 10$  [μs]; time to half-peak on surge wave tail  $t_p = 350$  [μs]. The values of other waveform parameters determined by equation (5) are shown in Table 2.

Tab. 2. Primary waveform parameters for a 100 [kA], 10/350 [μs] lightning discharge.

correction factor	$\eta$	-	0,93
fall time coefficient	$\tau_1$	μs	19
fall time coefficient	$\tau_1$	μs	485

The measure for total energy within a pulsation band  $0 \leq \omega \leq \omega_g$  is the quotient that can be calculated through the expression (6).

$$W_s / W = \int_0^{\omega_g} |I(\omega)|^2 d\omega / \int_0^{\infty} |I(\omega)|^2 d\omega \quad (6)$$

where:  $\omega_g$  – upper limit frequency (pulsation) of a lightning discharge pulse,  $I(\omega)$  – discharge current amplitude for individual pulse harmonics.

Reducing the pulse leading edge rise duration and the time to half-peak of the lightning discharge pulse waveform automatically increases

the bandwidth occupied by the entire signal spectrum. The values of these parameters impact the shape of separate signal spectrum fragments. The time to half-peak of a lightning discharge pulse determines the spectrum shape for relatively low frequencies (in the order of several dozen [kHz]), while the leading-edge duration determines the spectrum shape for a higher frequency range. When considering the propagation of electromagnetic waves originating from a lightning pulse, within an area with used ESS, one should take into account two propagation centres, where interference signals propagate:

- free space – propagation of an interfering electromagnetic wave associated with the lightning pulse depends on the frequency and components of this signal spectrum;
- propagation on an interfering electromagnetic wave inside buildings and building partitions – take into account the damping (screening) of such partitions, which is a function depending on the frequency and power of the signal associated with a lightning discharge pulse.

Screening of an interfering electromagnetic field, especially for interference induced through walls and building partitions [41,42], is an effect particularly known for the range of higher

frequencies and electric field intensity components  $E$  for the range of low frequencies. Lightning protection rod arranged much less frequently than rebars lead to reduced electromagnetic field inside buildings with utilized ESS. The achieved screening effects may be characterized using technical parameters associated with screening effectiveness  $S_E$ ,  $S_H$  (values related to electromagnetic field components, component  $E$ [V/m],  $H$ [A/m]). Fig. 6 shows the impact of various lightning protection net mesh size dimension on screening – electric field intensity  $E$  and magnetic field intensity  $H$ .

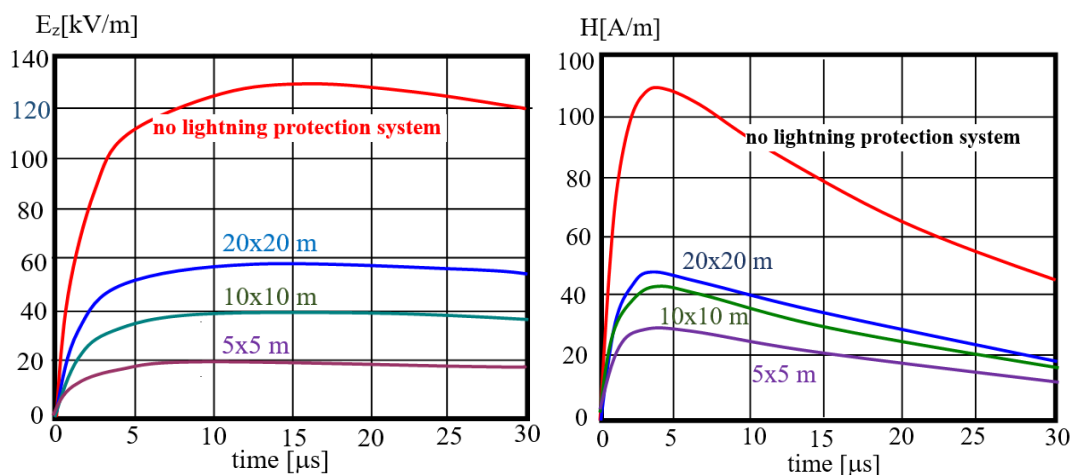


Fig. 6. Intensity waveforms: a) magnetic field intensity  $H$ , b) electric field intensity  $E$  within a building with installed ESS, for different mesh sizes of the lightning protection net, upon induction with a two-component discharge pulse with the parameters of 20 [kA], 2/25 [ $\mu$ s], where: maximum current value  $I_{max} = 20$  [kA],  $t_i = 2$  [ $\mu$ s] pulse leading edge duration,  $t_p = 25$  [ $\mu$ s] time to half-peak. The basic parameters of aperiodic primary channel discharge current pulse are determined for waveforms as shown in Fig. 7.

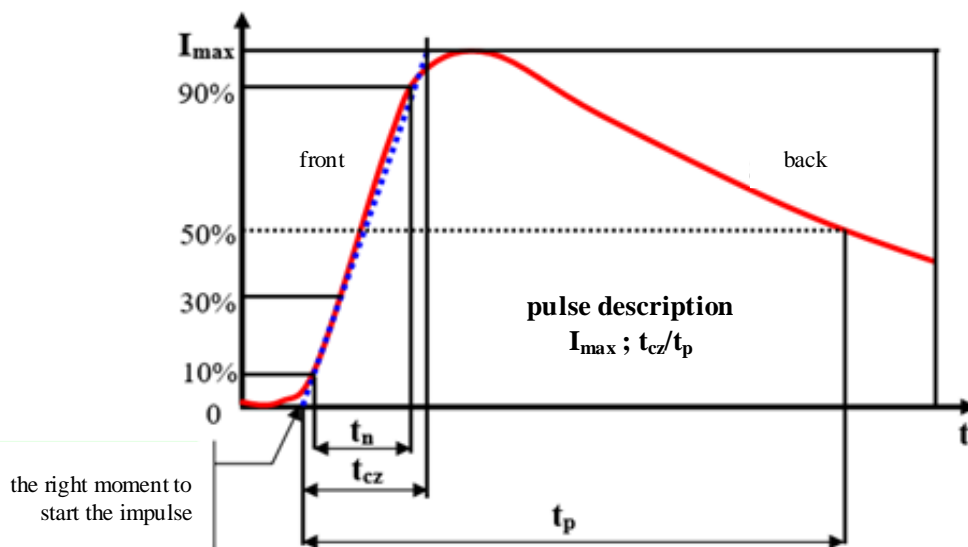


Fig. 7. Basic aperiodic pulse parameters – primary channel discharge current, where:  $I_{max}$  – maximum discharge current pulse,  $t_{cz}$  – pulse leading edge duration,  $t_p$  – discharge pulse time to half-peak,  $t_n$  – discharge pulse rise time,  $t_{cz}$  – discharge pulse leading edge duration,  $t_p$  – discharge pulse duration.

Arrangement diagram of protecting ESS against lightning discharge pulses in power supply lines and external circuits (e.g.,

sensors, signalling devices, antennas, detection circuits, etc.) reaching the Alarm Control Panel (ACP) is shown in Fig. 8.

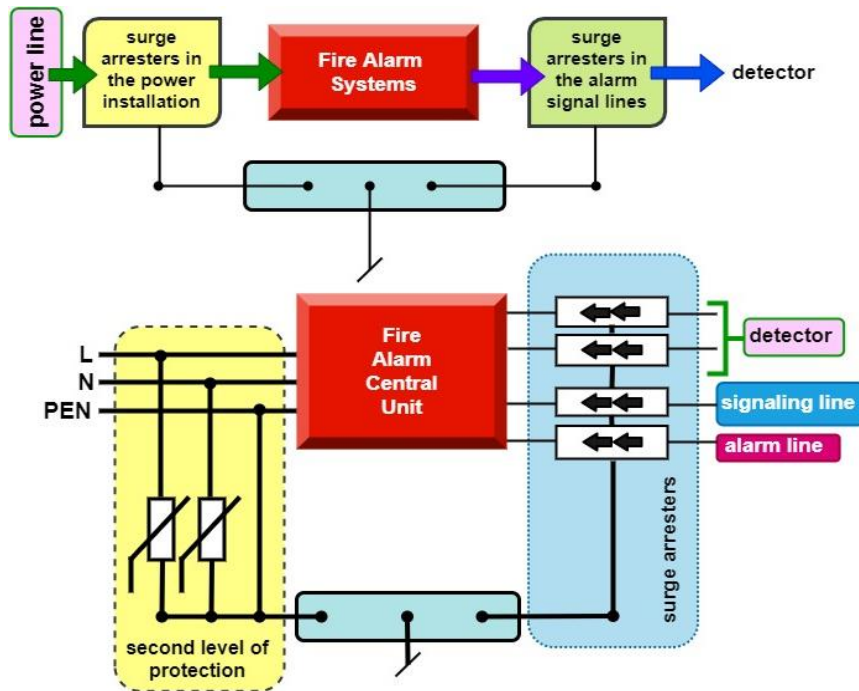


Fig. 8. Organization of ESS protection against lightning discharge pulses.

The peak value of overvoltage pulses in ESS depends on the environment where individual system devices or elements are installed. When assessing such an environment, the following should be taken into account:

- factors associated with the properties of the area where the ESS is installed, namely:
  - discharge surface density – developed maps,
  - resistivity of the soil on which a given building is set,
  - type of buildings in the vicinity of the protected facility, e.g., train station.
- degree of ESS exposure to lightning discharges:
  - probability of a lightning discharge pulse hitting the protected building,
  - method of laying power cables, detection circuits and loops for the building ESS,
  - method of laying power and signal cables reaching the protected building,
  - probability of a lightning discharge pulse hitting in close proximity to the building,
  - technical utilities around the protected building, e.g., buried metal reinforcement elements, rains, cable screens, etc.
- conditions inducted within the facilities protected by ESS:

- method of earthing and supplying ESS devices and elements [43,44];
- rules for routing and laying signal or power cables,
- the use of elements protecting against lightning discharge pulses – external or power lines or internal on detection circuits.

Lightning protection effectiveness for a building with installed ESS can be defined as the probability for a protective device, including lightning protection, surge arresters in power lines, detection circuits and railway traction systems, e.g., horn gaps – located every 600 [m] or 1200 [m] to absorb surge energy, preventing damage to the protected facility or given circuits. There are four protection levels, which correspond to different basic lightning current parameters. The protection level can also be defined in words, with such terms as “basic protection”, “strict protection” and “special protection” used in such a case. Fig. 9 shows simplified solutions in terms of powering ESS, and other electrical devices operated within a given building. ESS devices and elements are always supplied from separate electric circuits protected by a fuse.

The source literature assumes estimating that a risk of damaging modern ESS devices and systems may occur event at 1.5 [km] from the primary lightning discharge pulse channel.

The standard “IEC 61662:1995 Assessment of the Risk of Damage Due to Lightning” evaluates the risk of damage to electronic devices and systems at a distance of 500 [m] from the location of a lightning strike – lightning discharge pulse.

Overvoltage in a supply line for an ESS used within a building involves various possibilities of an electric shock – inducing a state of full or partial unfitness of a given system. Due to the parameters of interfering pulses propagating within power systems or detection circuits and loops, ESS can be exposed to conducted shock, inductive or capacitive coupling and electromagnetic radiation. There can also be a combination of different electromagnetic impacts for various frequency bands – low, average, or high, conducted electric shock – pulses in power lines, as well as, e.g., capacitive coupling and (or) radiation. The availability time  $T_D$  that may occur during the impact of a lightning discharge pulse, when it is still possible to

counteract a given shock, is a function that depends on overvoltage protections within the power line, as well as interference propagation paths to the outside or inside a facility.

For the case of a conducted interference in a building protected by an ESS, there are four protection categories with different limit voltages, which is shown in Fig. 9. In the event of an overvoltage pulse, individual protection degrees lead to reduced overvoltage amplitude that propagates along the power line. The interference amplitude originating from the overvoltage pulse is limited after being absorbed by individual “thresholds”. Some of the pulse energy is absorbed by existing limitation degrees. The use of four different ESS protection degrees leads to the availability time  $T_D$  within a system always greater than in the case of, e.g., using an arrester only on the power supply line.

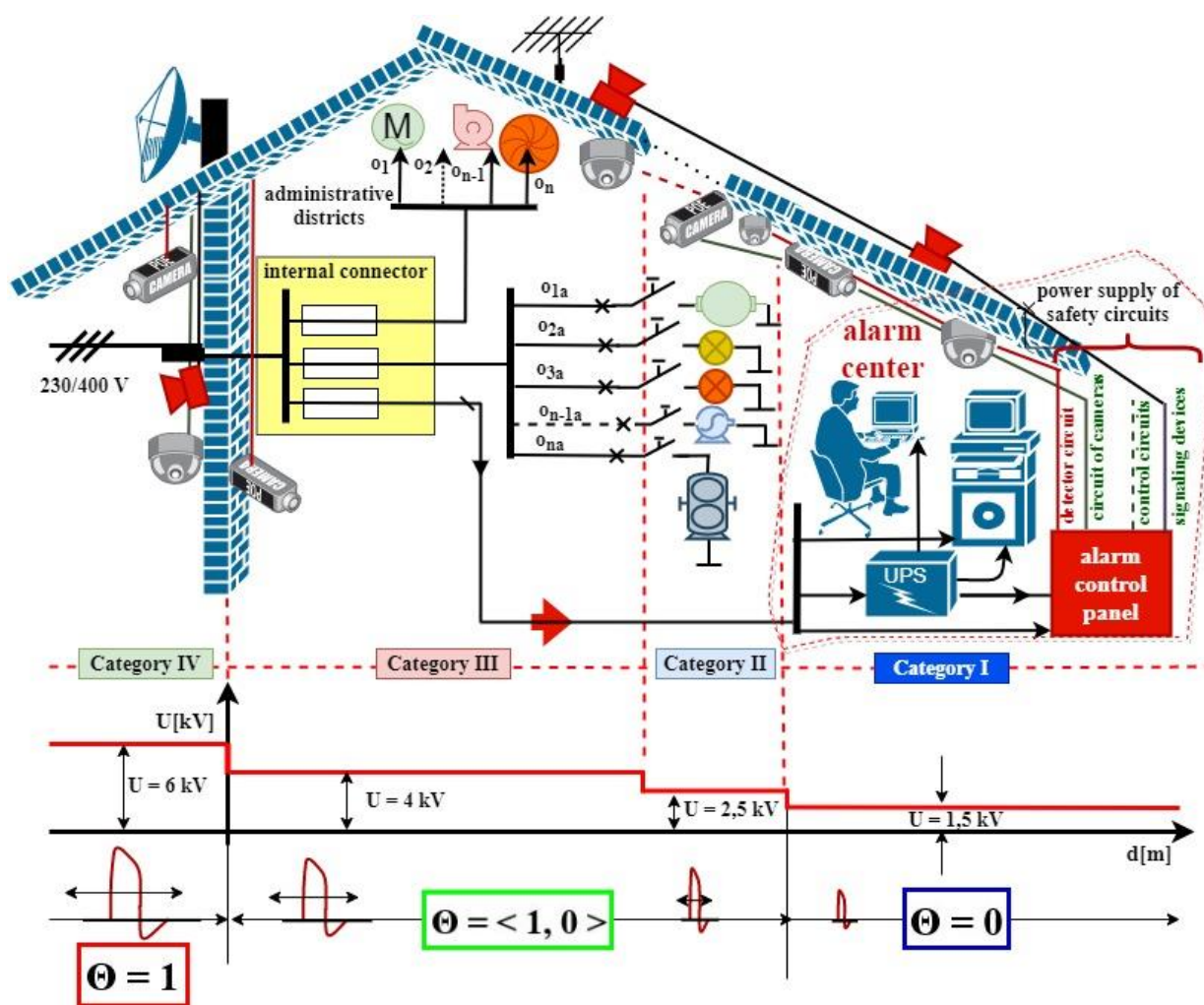


Fig. 9. Solution of the method for supplying ESS and other electric devices stored within a given building, where:  $o_{1a}, o_{2a}, \dots, o_{na}$ ;  $o_1, o_2, \dots, o_n$  – internal power lines (WLZ),  $\Theta$  – coefficient of lightning discharge pulse impact on electric devices and elements, including ESS.

### 3. Testing surge arresters

Surge arresters, among others, are used in order to protect electronic security systems against the impact of external natural interference. This is why the authors tested them. A diagram of a test bench for studying the electric surge immunity of PW-2-32 and PW-S surge arresters is shown in Fig.



Fig. 10. Test bench for studying electric surge immunity of a PW-2-32 and PW-S surge arrester.

A PW-S surge arrester is used to protect devices powered with  $\leq 230\text{V AC}$ , while a PW-2-32 is used for devices supplied with  $\leq 24\text{V DC}$ . The laboratory bench shown in Fig. 10 consists of a “surge” type pulse generator and pulse measuring equipment, i.e., an oscilloscope and an HV measuring probe. The measuring equipment has valid accredited calibration certificates that confirm the current metrological status.

A coupling–decoupling network with a resistance of  $40 [\Omega]$  and a capacitance of  $0.5 [\mu\text{F}]$  is used to study a PW-2-32 surge

arrester. The waveform of electric surge pulses at the generator output was generated in accordance with standard PN-EN 61000-4-5:2014 that applies testing various surge arresters used in actual systems [45]. Fig. 11 shows the rating plates of the arresters subject to the electric surge immunity test. Arrester rating plates contain basic technical data related to their use in power lines or systems.

arrester. The network is serially coupled to a pulse generator. The internal resistance of the generator is  $2 [\Omega]$ . Testing the immunity to electric surges is conducted in accordance with standard PN-EN 61000-4-5:2014. It is recommended for an EUT to be located at a distance of approx.  $0.5 [\text{m}]$  from the generator and placed on a non-metal,  $0.1 [\text{m}]$  high insulating base. The connecting cables cannot be laid on the reference ground, where the pulse generator is positioned.

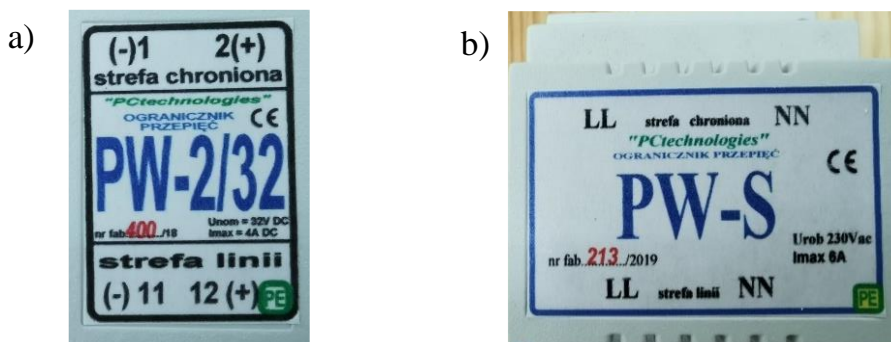


Fig. 11. Rating plates for studied surge arresters: a) PW-2-32, b) PW-S.

Fig. 12 shows an electric surge pulse at the generator output, in accordance with PN-EN 61000-4-5:2014 standard. The pulse reaches its maximum amplitude  $U = 2.015$  [kV], after  $t = 60$  [ $\mu$ s] reaches a value equal to zero, however the generator exhibits an oscillatory waveform – negative value appears, which after  $t = 120$  [ $\mu$ s] reaches a maximum amplitude  $U = 0.936$  [kV]. At the surge arrester input (Fig. 13) and after passing the forming

systems, the pulse reaches an amplitude  $U = 387.35$  [V], the rear pulse edge reaches  $U = 36$  [V] after  $t = 37.5$  [ $\mu$ s]. Fig. 14 shows an electric surge pulse after leaving an unloaded PW-2-32 surge arrester, for an exposure value of  $+2$  [kV]. The maximum limited voltage value is  $U = 38$  [V] and is maintained on the element (arrester) for  $\Delta t = 33$  [ $\mu$ s]. On the element output, after  $\Delta t = 39$  [ $\mu$ s] – voltage limitation is equal to zero.

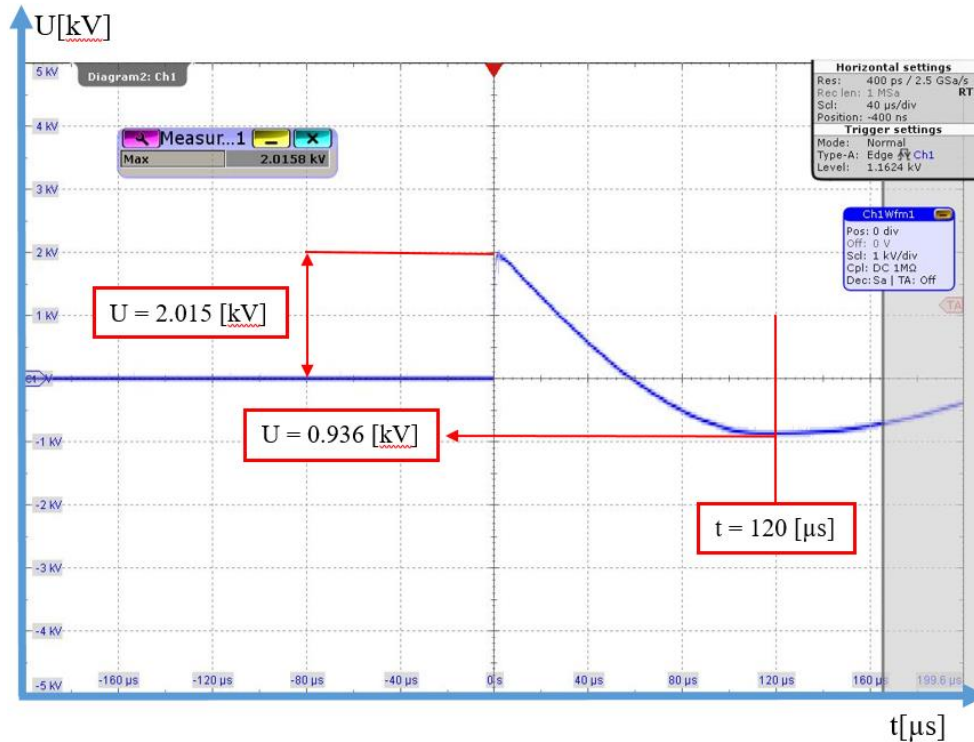


Fig. 12. Electric surge pulse at the generator output, in accordance with standard PN-EN 61000-4-5:2014.

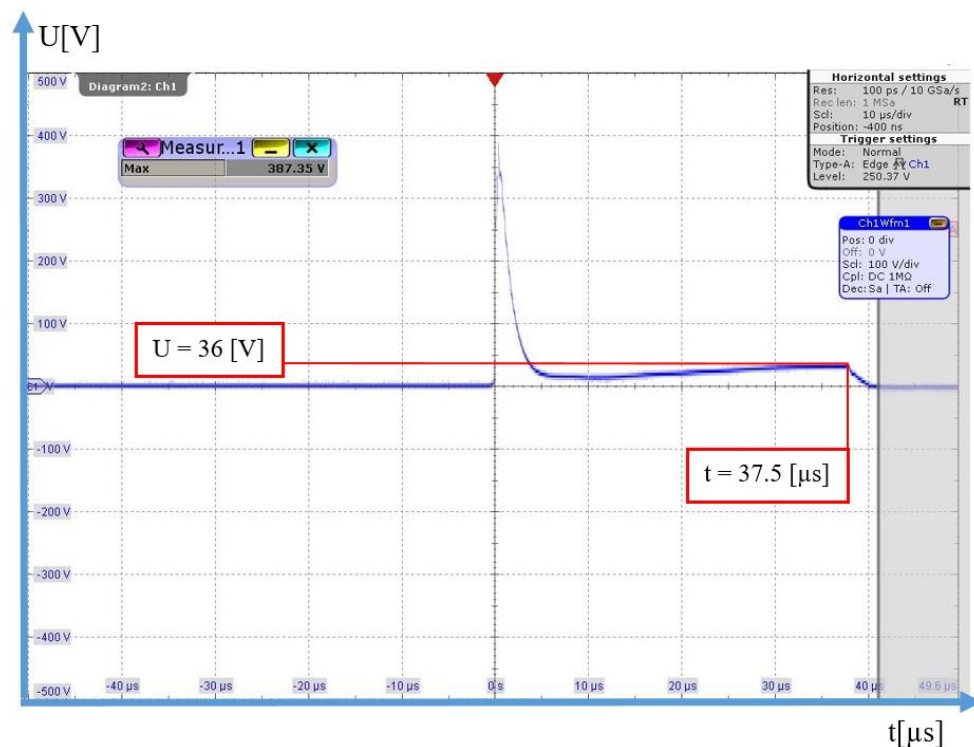


Fig. 13. Electric surge pulse at the input of a PW-2-32 surge arrester, exposure value  $+2$  [kV].

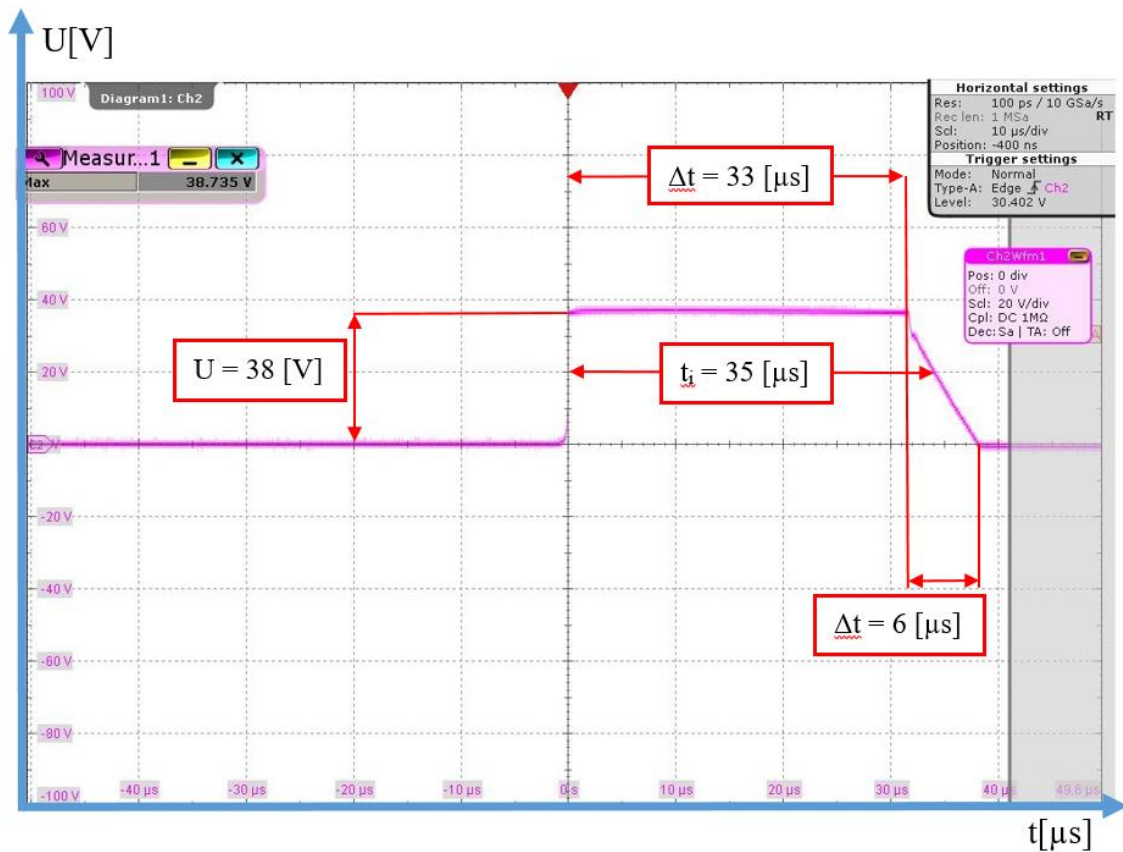


Fig. 14. Electric surge pulse at the input of an unloaded PW-2-32 surge arrester, exposure value +2 [kV].

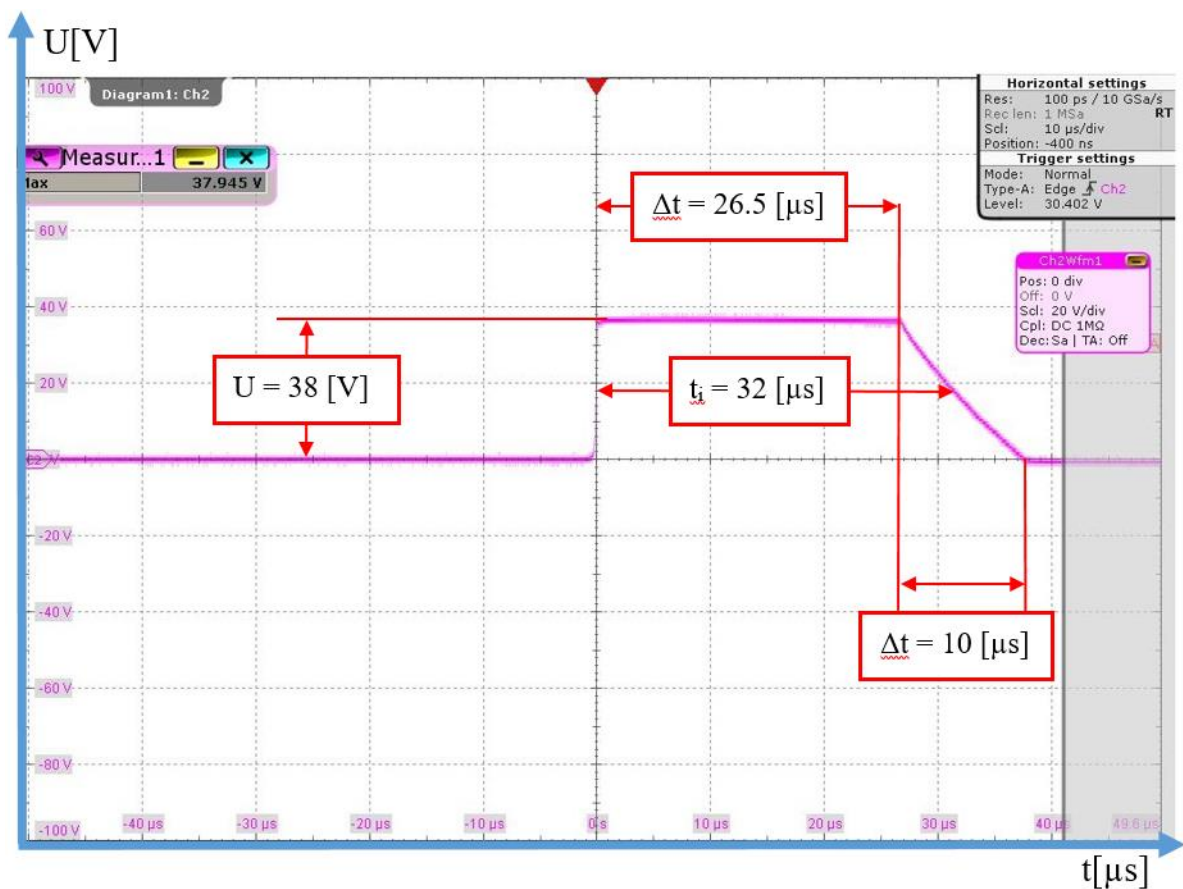


Fig. 15. Electric surge pulse at the input of a PW-2-32 surge arrester with a load of 50 [Ω], exposure value +2 [kV].

Fig. 14 and 15 shows electric surge pulses at the input of a PW-2-32 surge arrester that is unloaded (Fig. 14), and with a 50 [Ω] load (Fig. 15) for a constant exposure value of +2 [kV]. The presented graphs clearly indicate the impact of load resistance on the waveform of a surge pulse after passing

Tab. 3. Comparison of waveform parameters for electric surge pulse at the output of a PW-2-32 surge arrester, with a 50 [Ω] load and unloaded.

Arrester with a 50 Ω load			Arrester without load		
Time parameters [μs]	Pulse duration for a constant amplitude value	26.5	Time parameters [μs]	Pulse duration for a constant amplitude value	33
	Pulse decay – fall time	10		Pulse decay – fall time	6
Pulse amplitude [V]	38		Pulse amplitude [V]	38	

Loading a PW-2-32 surge arrester with a resistance of 50 [Ω] leads to reduced pulse duration for a constant amplitude value, and changes the system's time constant. However, the pulse decay – fall time is reduced for an unloaded system – lower time constant in the system – almost twofold. Pulse amplitude value

through an arrester. The pulse duration  $t_i$ , duration for a constant pulse amplitude and the pulse decay – fall time are changed. The waveform parameters for electric surge pulse at the output of a PW-2-32 surge arrester, with a 50 [Ω] load and unloaded, is included in Table 3.

is at a constant level equal to 38 [V].

Fig. 16-19 shows electric surge pulses at the output of the generator and out of a PW-S surge arrester that is unloaded (Fig. 18) and with a 50 [Ω] load (Fig. 19), for a constant exposure value of 4 [kV].

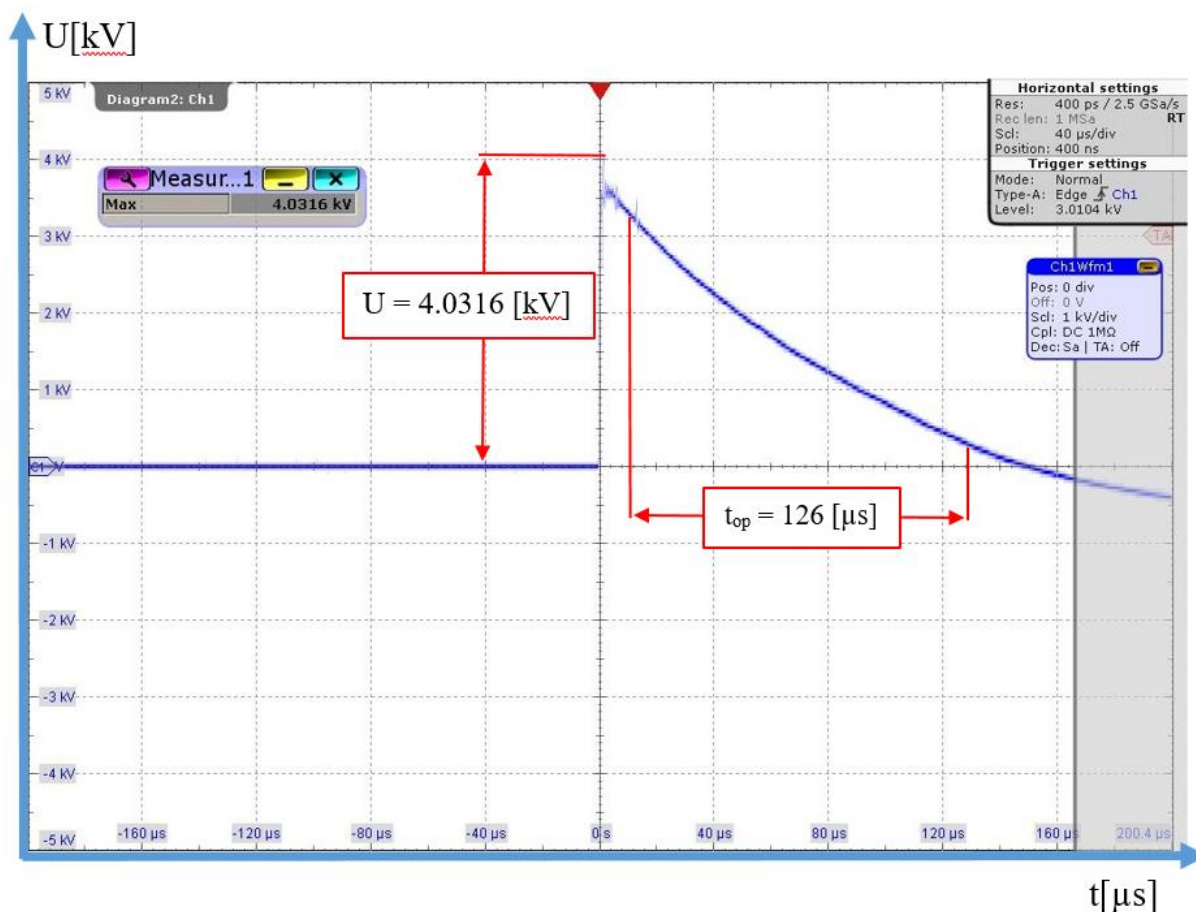


Fig. 16. Electric surge pulse at the generator output, in accordance with standard PN-EN 61000-4-5:2014, exposure value +4 [kV].

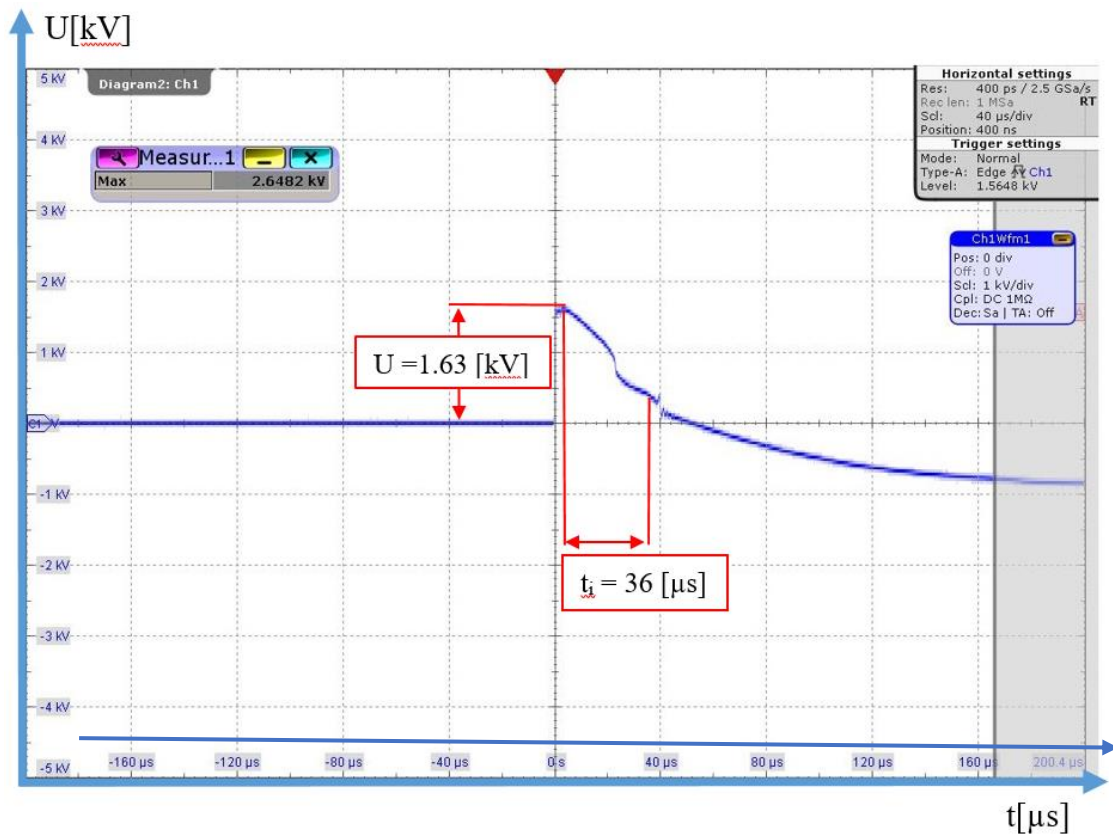


Fig. 17. Electric surge pulse at the input of a PW-S surge arrester, exposure value 4 [kV].

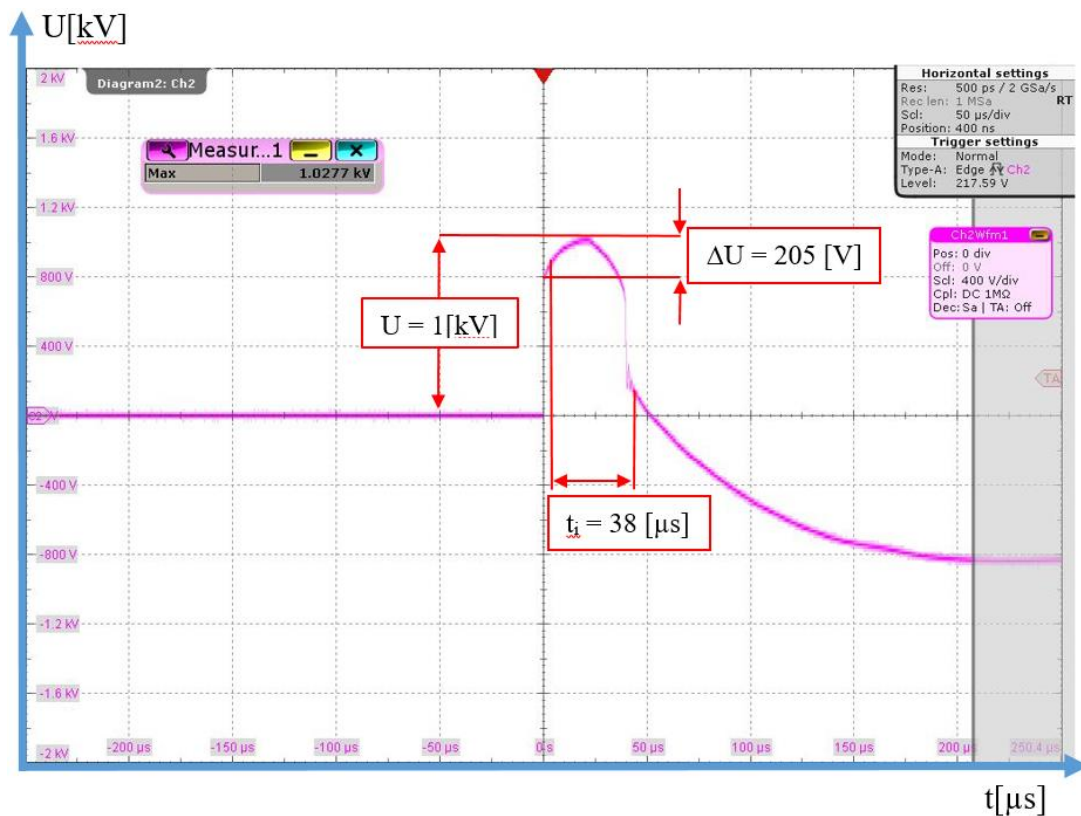


Fig. 18. Electric surge pulse at the output of an unloaded PW-S surge arrester, exposure value 4 [kV].

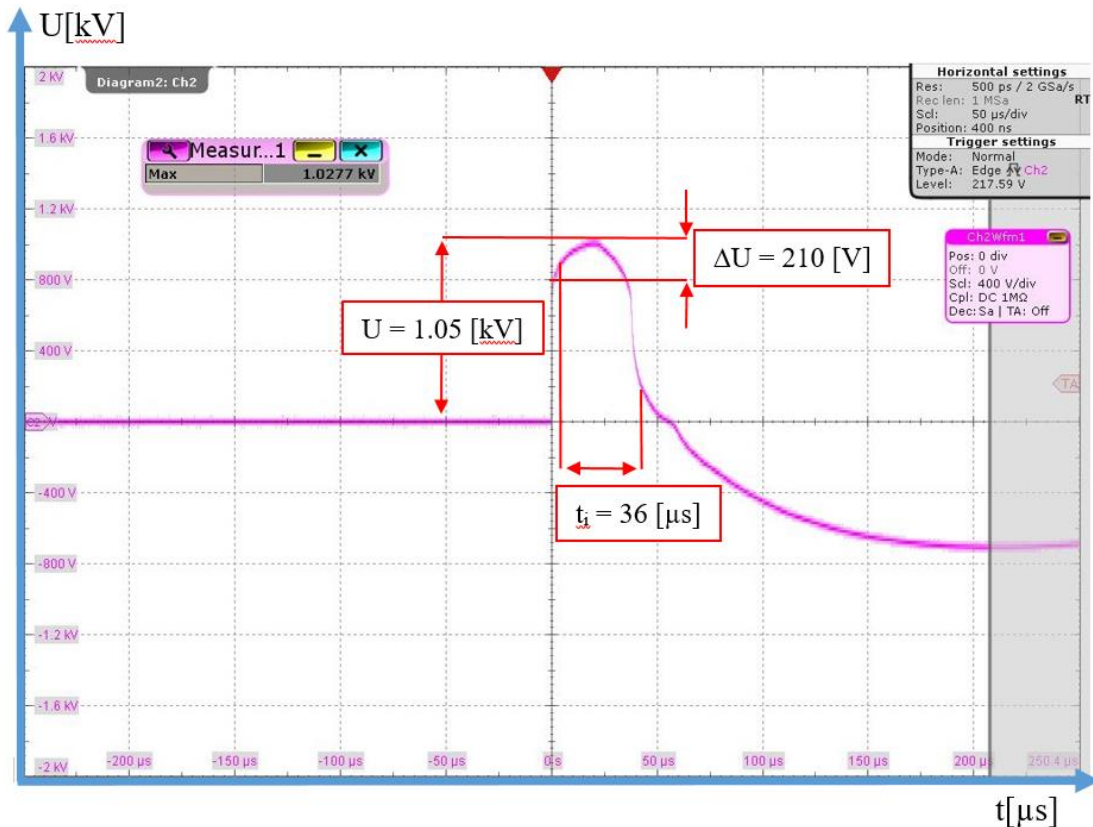


Fig. 19. Electric surge pulse at the input of a PW-S surge arrester with a load of 50 Ω, exposure value 4 [kV].

The presented graphs clearly indicate the impact of load resistance on the waveform of a surge pulse after passing through an arrester. The  $t_i$  pulse duration is changed.

Comparison of electric surge pulse waveforms on the output of a PW-S surge arrester with and without a 50 [Ω] load are shown in Table 4.

Tab. 4. Comparison of electric surge pulse waveforms on the output of a PW-S surge arrester with and without a 50 [Ω] load.

Arrester with a 50 [Ω] load			Arrester without load		
Time parameters [μs]	Pulse duration	36	Time parameters [μs]	Pulse duration	38
Pulse amplitude [kV]	1.05		Pulse amplitude [V]	1	
Pulse amplitude increment [ΔV w V]	210		Pulse amplitude increment [ΔV]	205	

Loading a PW-S surge arrester with a resistance of 50 [Ω] leads to reduced pulse duration. The output pulse waveform experiences an increase in the pulse amplitude  $\Delta V$ , which depends on the load.

#### 4. Reliability and operational analysis of the power supply in electronic security systems of intelligent buildings taking into account external natural interference

The operating process of the aforementioned systems involves interference in the operation of such devices or elements (e.g., sensors) that can cause the occurrence of four various operating states, which are a function of the amplitude of such interference – intended or unintended, internal or external (stationary or

mobile). The following system operating states can be distinguished:

- state  $S_{PZ}$  – interference amplitude (level) is low, all systems are functioning correctly,
- state  $S_{ZB1}$  – interference amplitude (level) is high, however elements fitted in systems and devices automatically eliminate, e.g., voltages through the used electronic elements or passive filters, as well as active or existing screening,
- state  $S_{ZB2}$  – interference amplitude (level) is high, system(s) pass from the state of  $S_{PZ}$  or  $S_{ZB1}$  to a state of partial unfitness –  $S_{ZB2}$ , restoration of fitness states requires intervention of ARC maintenance or service personnel,

- state  $S_B$  – interference amplitude (level) is very high – e.g., atmospheric overvoltage or one associated with commutation in a power grid or a power line short-circuit – management systems within an intelligent system pass into an unfitness state  $S_B$ . Restoring the state of full or partial

fitness requires intervention of the ARC maintenance or service personnel.

Fig. 20 shows a graph of transition for an event of ESS hit by a lightning pulse.

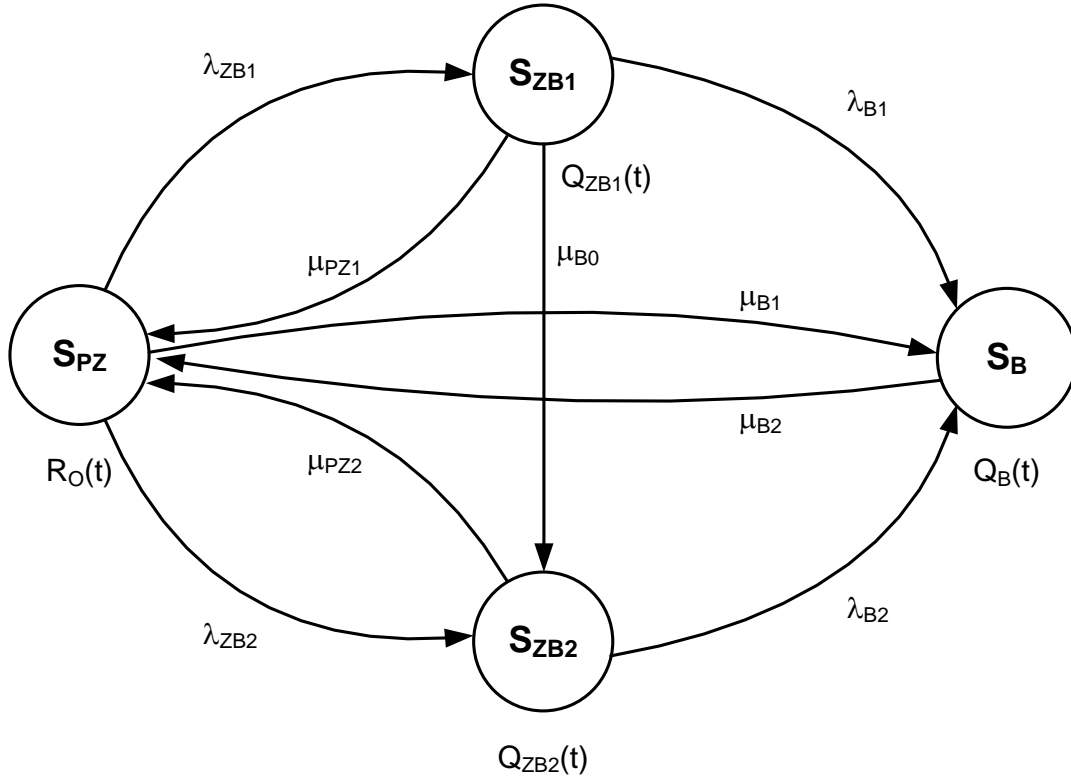


Fig. 20. ESS relations in terms of reliability and operation.

Designations in Fig.:

$R_0(t)$  – probability function of the system staying in the state of full fitness  $S_{PZ}$ ,

$Q_{ZB1}$  – the probability function of a system staying in a state of partial fitness I  $S_{ZB1}$ ,

$Q_{ZB2}$  – the probability function of a system staying in a state of partial fitness II  $S_{ZB2}$ ,

$Q_B(t)$  – the probability function of a system staying in a state of unfitness  $S_B$ ,

$\lambda_{ZB1}$  – intensities of transition from a state of full fitness  $S_{PZ}$  to partial fitness I  $S_{ZB1}$ ,

$\lambda_{ZB2}$  – intensities of transition from a state of full fitness  $S_{PZ}$  to partial fitness II  $S_{ZB2}$ ,

$\mu_{PZ1}$  – intensities of transition from a state of partial fitness I  $S_{ZB1}$  to full fitness  $S_{PZ}$ ,

$\mu_{PZ2}$  – intensities of transition from a state of partial fitness II  $S_{ZB2}$  to full fitness  $S_{PZ}$ ,

$\mu_{B0}$  – intensities of transition from a state of partial fitness I

$S_{ZB1}$  to partial fitness II  $S_{ZB2}$ ,

$\mu_{B1}$  – intensities of transition from a state of full fitness  $S_{PZ}$  to unfitness  $S_B$ ,

$\mu_{B2}$  – intensities of transition from a state of unfitness  $S_B$  to full fitness  $S_{PZ}$ ,

$\lambda_{B1}$  – intensities of transition from a state of partial fitness I  $S_{ZB1}$  to unfitness  $S_B$ ,

$\lambda_{B2}$  – intensities of transition from a state of partial fitness II  $S_{ZB2}$  to unfitness  $S_B$ .

Intensities of transition  $\lambda_{ZB1}$ ,  $\lambda_{ZB2}$ ,  $\lambda_{B1}$ ,  $\lambda_{B2}$ ,  $\mu_{B0}$  and  $\mu_{B1}$  depend on, among others, the effectiveness of applied solutions that ensure adequate overvoltage protection.

The system shown in Fig. 20 can be described by the following Chapman–Kolmogorov equations:

$$R'_0(t) = -\lambda_{ZB1} \cdot R_0(t) + \mu_{PZ1} \cdot Q_{ZB1}(t) - \lambda_{ZB2} \cdot R_0(t) + \mu_{PZ2} \cdot Q_{ZB2}(t) - \mu_{B1} \cdot R_0(t) + \mu_{B2} \cdot Q_B(t)$$

$$\begin{aligned}
Q'_{ZB1}(t) &= \lambda_{ZB1} \cdot R_0(t) - \mu_{PZ1} \cdot Q_{ZB1}(t) - \lambda_{B1} \cdot Q_{ZB1}(t) \\
&\quad - \mu_{B0} \cdot Q_{ZB1}(t) \\
Q'_{ZB2}(t) &= \lambda_{ZB2} \cdot R_0(t) - \mu_{PZ2} \cdot Q_{ZB2}(t) - \lambda_{B2} \cdot Q_{ZB2}(t) \\
&\quad + \mu_{B0} \cdot Q_{ZB1}(t) \\
Q'_B(t) &= \lambda_{B1} \cdot Q_{ZB1}(t) + \lambda_{B2} \cdot Q_{ZB2}(t) + \mu_{B1} \cdot R_0(t) - \mu_{B2} \\
&\quad \cdot Q_B(t)
\end{aligned} \tag{7}$$

Assuming the baseline conditions:

$$R_0(0) = 1, \quad Q_{ZB1}(0) = Q_{ZB2}(0) = Q_B(0) = 0 \tag{8}$$

and applying the Laplace transform, the following system of linear equations is obtained:

$$\begin{aligned}
s \cdot R_0^*(s) - 1 &= -\lambda_{ZB1} \cdot R_0^*(s) + \mu_{PZ1} \cdot Q_{ZB1}^*(s) - \lambda_{ZB2} \\
&\quad \cdot R_0^*(s) + \mu_{PZ2} \cdot Q_{ZB2}^*(s) - \mu_{B1} \cdot R_0^*(s) \\
&\quad + \mu_{B2} \cdot Q_B^*(s) \\
s \cdot Q_{ZB1}^*(s) &= \lambda_{ZB1} \cdot R_0^*(s) - \mu_{PZ1} \cdot Q_{ZB1}^*(s) - \lambda_{B1} \cdot Q_{ZB1}^*(s) \\
&\quad - \mu_{B0} \cdot Q_{ZB1}^*(s) \\
s \cdot Q_{ZB2}^*(s) &= \lambda_{ZB2} \cdot R_0^*(s) - \mu_{PZ2} \cdot Q_{ZB2}^*(s) - \lambda_{B2} \cdot Q_{ZB2}^*(s) \\
&\quad + \mu_{B0} \cdot Q_{ZB1}^*(s) \\
s \cdot Q_B^*(s) &= \lambda_{B1} \cdot Q_{ZB1}^*(s) + \lambda_{B2} \cdot Q_{ZB2}^*(s) + \mu_{B1} \cdot R_0^*(s) - \\
&\quad \mu_{B2} \cdot Q_B^*(s)
\end{aligned} \tag{9}$$

Transforming it, a record in the schematic view is obtained:

$$\begin{aligned}
R_0^*(s) &= -\frac{b_1 \cdot b_2 \cdot c}{b_1 \cdot b_2 \cdot \mu_{B1} \cdot \mu_{B2} - a \cdot b_1 \cdot b_2 \cdot c + b_2 \cdot c \cdot \lambda_{ZB1} \cdot \mu_{PZ1} + b_1 \cdot c \cdot \lambda_{ZB2} \cdot \mu_{PZ2} + \\
&\quad + b_2 \cdot \lambda_{B1} \cdot \mu_{B2} \cdot \lambda_{ZB1} + b_1 \cdot \lambda_{B2} \cdot \mu_{B2} \cdot \lambda_{ZB2} + c \cdot \mu_{B0} \cdot \lambda_{ZB1} \cdot \mu_{PZ2} + \\
&\quad + \mu_{B0} \cdot \lambda_{B2} \cdot \mu_{B2} \cdot \lambda_{ZB1}} \\
Q_{ZB1}^*(s) &= -\frac{b_2 \cdot c \cdot \lambda_{ZB1}}{b_1 \cdot b_2 \cdot \mu_{B1} \cdot \mu_{B2} - a \cdot b_1 \cdot b_2 \cdot c + b_2 \cdot c \cdot \lambda_{ZB1} \cdot \mu_{PZ1} + b_1 \cdot c \cdot \lambda_{ZB2} \cdot \mu_{PZ2} + \\
&\quad + b_2 \cdot \lambda_{B1} \cdot \mu_{B2} \cdot \lambda_{ZB1} + b_1 \cdot \lambda_{B2} \cdot \mu_{B2} \cdot \lambda_{ZB2} + c \cdot \mu_{B0} \cdot \lambda_{ZB1} \cdot \mu_{PZ2} + \\
&\quad + \mu_{B0} \cdot \lambda_{B2} \cdot \mu_{B2} \cdot \lambda_{ZB1}} \\
Q_{ZB2}^*(s) &= -\frac{b_1 \cdot c \cdot \lambda_{ZB2} + c \cdot \mu_{B0} \cdot \lambda_{ZB1}}{b_1 \cdot b_2 \cdot \mu_{B1} \cdot \mu_{B2} - a \cdot b_1 \cdot b_2 \cdot c + b_2 \cdot c \cdot \lambda_{ZB1} \cdot \mu_{PZ1} + b_1 \cdot c \cdot \lambda_{ZB2} \cdot \mu_{PZ2} + \\
&\quad + b_2 \cdot \lambda_{B1} \cdot \mu_{B2} \cdot \lambda_{ZB1} + b_1 \cdot \lambda_{B2} \cdot \mu_{B2} \cdot \lambda_{ZB2} + c \cdot \mu_{B0} \cdot \lambda_{ZB1} \cdot \mu_{PZ2} + \\
&\quad + \mu_{B0} \cdot \lambda_{B2} \cdot \mu_{B2} \cdot \lambda_{ZB1}} \\
Q_B^*(s) &= -\frac{b_1 \cdot b_2 \cdot \mu_{B1} + b_2 \cdot \lambda_{B1} \cdot \lambda_{ZB1} + b_1 \cdot \lambda_{B2} \cdot \lambda_{ZB2} + \mu_{B0} \cdot \lambda_{B2} \cdot \lambda_{ZB1}}{b_1 \cdot b_2 \cdot \mu_{B1} \cdot \mu_{B2} - a \cdot b_1 \cdot b_2 \cdot c + b_2 \cdot c \cdot \lambda_{ZB1} \cdot \mu_{PZ1} + b_1 \cdot c \cdot \lambda_{ZB2} \cdot \mu_{PZ2} + \\
&\quad + b_2 \cdot \lambda_{B1} \cdot \mu_{B2} \cdot \lambda_{ZB1} + b_1 \cdot \lambda_{B2} \cdot \mu_{B2} \cdot \lambda_{ZB2} + c \cdot \mu_{B0} \cdot \lambda_{ZB1} \cdot \mu_{PZ2} + \\
&\quad + \mu_{B0} \cdot \lambda_{B2} \cdot \mu_{B2} \cdot \lambda_{ZB1}}
\end{aligned} \tag{10}$$

where:

$$\begin{aligned}
a &= s + \lambda_{ZB1} + \lambda_{ZB2} + \mu_{B1} \\
b_1 &= s + \mu_{PZ1} + \lambda_{B1} + \mu_{B0} \\
b_2 &= s + \mu_{PZ2} + \lambda_{B2} \\
c &= s + \mu_{B2}
\end{aligned}$$

By conducting further mathematical analysis, we obtain relationships, which allow calculating the probabilities of a system staying in states of full fitness  $S_{PZ}$ , partial fitness  $S_{ZB1}$  and  $S_{ZB2}$ , and unfitness  $S_B$ .

## 5. Modelling a reliability and operational process for the power supply continuity in electronic security systems of intelligent buildings taking into account external natural interference

Simulation and computer methods make it possible to determine the impact of changes in the indicators specifying the effectiveness of applies overvoltage protection solutions on the readiness of the entire system [46-51].

The authors conducted computer-aided calculations enabling the determination of the probability for a system staying in the state of full fitness. Such a procedure is shown in the following example.

### Example

Let us assume the following values describing the analysed system:

- research duration – 1 year (the value of this time is given in the units as hours [h]):  $t = 8760$  [h]
- intensity of transitions from a state of full fitness to partial fitness I  $\lambda_{ZB1}$ :  $\lambda_{ZB1} = 0,000001$   $\left[\frac{1}{h}\right]$
- intensity of transitions from a state of full fitness to partial fitness II  $\lambda_{ZB2}$ :  $\lambda_{ZB2} = 0,0000001$   $\left[\frac{1}{h}\right]$
- intensity of transitions from a state of partial fitness I to unfitness  $\lambda_{B1}$ :  $\lambda_{B1} = 0,0000001$   $\left[\frac{1}{h}\right]$
- intensity of transitions from a state of partial fitness II to unfitness  $\lambda_{B2}$ :  $\lambda_{B2} = 0,000001$   $\left[\frac{1}{h}\right]$
- intensity of transitions from a state of partial fitness I to full fitness II  $\mu_{B0}$ :  $\mu_{B0} = 0,00000001$   $\left[\frac{1}{h}\right]$
- intensity of transitions from a state of full fitness to unfitness  $\mu_{B1}$ :  $\mu_{B1} = 0,00000001$   $\left[\frac{1}{h}\right]$
- intensity of transitions from a state of unfitness to full fitness  $\mu_{B2}$ :  $\mu_{B2} = 0,001$   $\left[\frac{1}{h}\right]$
- intensity of transitions from a state of partial fitness I to full

fitness  $\mu_{PZ1}$ :  $\mu_{PZ1} = 0,1 \left[ \frac{1}{h} \right]$

- intensity of transitions from a state of partial fitness II to

full fitness  $\mu_{PZ2}$ :  $\mu_{PZ2} = 0,2 \left[ \frac{1}{h} \right]$

The following is obtained for the above input values, using the equation (10):

$R_0(s)$

$$\begin{aligned} & 1,110011 \cdot 10^{14} \cdot s + 1 \cdot 10^{14} \cdot \mu_{PZ1} + 1,1 \cdot 10^{13} \cdot \mu_{PZ2} + 1 \cdot 10^{22} \cdot s^2 \cdot \mu_{PZ1} + \\ & + 1 \cdot 10^{22} \cdot s^2 \cdot \mu_{PZ2} + 1,000111 \cdot 10^{20} \cdot s^2 + 1 \cdot 10^{22} \cdot s^3 + \\ & + 1,0001 \cdot 10^{20} \cdot s \cdot \mu_{PZ1} + 1,000011 \cdot 10^{20} \cdot s \cdot \mu_{PZ2} + \\ & + 1 \cdot 10^{20} \cdot \mu_{PZ1} \cdot \mu_{PZ2} + 1 \cdot 10^{22} \cdot s \cdot \mu_{PZ1} \cdot \mu_{PZ2} + 1,1 \cdot 10^7 \\ = & \frac{1,13101221 \cdot 10^8 \cdot s + 1,000111 \cdot 10^{20} \cdot s^2 \cdot \mu_{PZ1} + 1,000112 \cdot 10^{20} \cdot s^2 \cdot \mu_{PZ2} + \\ & + 1 \cdot 10^{22} \cdot s^3 \cdot \mu_{PZ1} + 1 \cdot 10^{22} \cdot s^3 \cdot \mu_{PZ2} + 2,21013421 \cdot 10^{14} \cdot s^2 + \\ & + 1,000222 \cdot 10^{20} \cdot s^3 + 1 \cdot 10^{22} \cdot s^4 + 1,100011 \cdot 10^{14} \cdot s \cdot \mu_{PZ1} + \\ & + 1,11001011 \cdot 10^{14} \cdot s \cdot \mu_{PZ2} + 1,000001 \cdot 10^{20} \cdot s \cdot \mu_{PZ1} \cdot \mu_{PZ2} + \\ & + 1 \cdot 10^{22} \cdot s^2 \cdot \mu_{PZ1} \cdot \mu_{PZ2}} \end{aligned}$$

As a result of transformations, we obtain:

$$\begin{aligned} R_0(t) = & 0,000001 \cdot e^{-0,01 \cdot t} + 5,00004171 \cdot 10^{-7} \\ & \cdot e^{-0,2000011 \cdot t} + 0,00000999986 \\ & \cdot e^{-0,1000011 \cdot t} + 0,99998849 \end{aligned}$$

As a final result, we get:  $R_0 = 0,9999885$

The presented reliability and operational analysis of the system enables a numerical evaluation of various types of overvoltage protection solutions. This enables their rational implementation in order to minimize the impact of interference on system operation.

## 6. Conclusions

Electronic security systems used to improve the security level

for people and property operate under varying environmental conditions. They are exposed to, among others, the impact of external and internal natural and artificial interference, which pose a significant threat to their correct operation. This is why elements or devices are used to ensure adequate overvoltage protection. They enable reducing the negative impact of external and internal interference on the operation of electronic devices, which has been confirmed in actual tests conducted by the authors. The conducted reliability and operational modelling confirmed the legitimacy of applying overvoltage protection.

Comprehensive scientific deliberations and the conducted actual tests enable developing an original method for assessing the power supply continuity in electronic security systems of intelligent buildings, taking into account external and internal natural or artificial interference (e.g., short-circuit in power lines, uncoupling a high-power electric motor from the mains). This method can be applied to evaluate power supply continuity also for other electronic devices. The considerations presented in the research paper allow a numerical evaluation of various solutions (technical and organizational ones) that can be used in order to mitigate the impact of external and internal natural interference on the functioning of electronic devices. This facilitates a rational implementation of overvoltage protections. In the course of further research involving this issue, the authors plan an analysis that enables assessing the effectiveness degree of the overvoltage protections of other elements and devices.

## References

1. Fischer R.J., Halibozek E.P., Walters D.C. Introduction to Security. Butterworth-Heinemann, 2019. <https://doi.org/10.1016/C2015-0-04068-0>
2. Kierzkowski A., Kisiel T. Simulation model of security control system functioning: A case study of the Wroclaw Airport terminal. Journal of Air Transport Management, 64 (B), 173-185 (2016). <https://doi.org/10.1016/j.jairtraman.2016.09.008>
3. Kierzkowski A., Kisiel T., Uchroński P.: Simulation Model of Airport Security Lanes with Power Consumption Estimation. Energies, 14, 6725, 2021. <https://doi.org/10.3390/en14206725>
4. Lewandowski J., Młynarski S., Pilch R., Smolnik M., Szybka J., Wiązania G.: An evaluation method of preventive renewal strategies of railway vehicles selected parts. Eksploatacja i Niezawodność – Maintenance and Reliability, 23 (4), 2021. <https://doi.org/10.17531/ein.2021.4.10>
5. Hu X., Zhou S., Chen T., Ghiasi M. Optimal energy management of a DC power traction system in an urban electric railway network with dogleg method, Energy Sources, Part A: Recovery, Utilization, and Environmental Effects, 2021, DOI: [10.1080/15567036.2021.1877373](https://doi.org/10.1080/15567036.2021.1877373)
6. Kochan A., Daszczyk W. B., Grabski W., Karolak, J. Formal Verification of the European Train Control System (ETCS) for Better Energy Efficiency Using a Timed and Asynchronous Model. Energies, 16, 8, 2023. <https://doi.org/10.3390/en16083602>
7. Jacyna M., Szczepański E., Izdebski M., Jasiński, S., Maciejewski M. Characteristics of event recorders in Automatic Train Control systems. Archives of Transport, 2018, 46, 61–70, doi:10.5604/01.3001.0012.2103.
8. Kukulski J., Jacyna M., Gołębiowski P. Finite Element Method in Assessing Strength Properties of a Railway Surface and Its Elements.

- Symmetry, 11, 1014, 2019. DOI: 10.3390/sym11081014
9. Klimczak T., Paś, J. Selected issues of the reliability and operational assessment of a fire alarm system. *Eksplatacja i Niezawodność – Maintenance and Reliability*, 21(4), 553–561, 2019. DOI: 10.17531/ein.2019.4.3.
  10. Perka B. The dissipation of electricity in electric cables under the influence of fire temperatures. *Przegląd Elektrotechniczny*, t. 97, 6, 2021, s. 105–108, <https://doi.org/10.15199/48.2021.06.19>
  11. Ott H. W. *Electromagnetic compatibility engineering*. Wiley. 2009. <http://dx.doi.org/10.1002/9780470508510>
  12. Si T., Xie S., Ji Z., Ma C., Wu Z., Wu J., Wang J. Synergistic effects of carbon black and steel fibers on electromagnetic wave shielding and mechanical properties of graphite/cement composites. *Journal of Building Engineering*, 45, 2022. <https://doi.org/10.1016/j.jobbe.2021.103561>
  13. Smolenski R., Lezynski P., Bojarski J., Drozd W., Choon Long L. Electromagnetic compatibility assessment in multiconverter power systems – Conducted interference issues. *Measurement*, vol. 165, pp. 108119, 2020. <https://doi.org/10.1016/j.measurement.2020.108119>
  14. Paś J., Rosiński A., Bialek K. A reliability-operational analysis of a track-side CCTV cabinet taking into account interference. *Bulletin of the Polish Academy of Sciences-Technical Sciences*, vol. 69(2), 2021, Article number: e136747. pp. 1-11. <https://doi.org/10.24425/bpasts.2021.136747>
  15. Paś J., Klimczak T., Rosiński A., Stawowy M. The Analysis of the Operational Process of a Complex Fire Alarm System Used in Transport Facilities. *Building Simulation*, vol. 15, issue 4, 2022. <https://doi.org/10.1007/s12273-021-0790-y>
  16. Pas J., Rosinski A., Chrzan M., Bialek K. Reliability-operational analysis of the LED lighting module including electromagnetic interference. *IEEE Trans. Electromagn. Compat.* 2020, 62, 2747–2755, doi:10.1109/temc.2020.2987388
  17. Khraisat A., Alazab A. A critical review of intrusion detection systems in the internet of things: techniques, deployment strategy, validation strategy, attacks, public datasets and challenges. *Cybersecurity*, 4, 18, 2021. <https://doi.org/10.1186/s42400-021-00077-7>
  18. Polak R., Laskowski, D., Matyszkiewicz R., Łubkowski P., Konieczny Ł., Burdzik R. Optimizing the Data Flow in a Network Communication between Railway Nodes. In *Research Methods and Solutions to Current Transport Problems*; Siergiejezyk, M., Krzykowska, K., Eds.; Springer: Cham, Switzerland, 2020; pp. 351–362. DOI: 10.1007/978-3-030-27687-4\_35.
  19. Yan H., Ma L., Zhao T., Zhang J. Research on repair method of abnormal energy consumption data of lighting and plug based on similar features. *Energy and Buildings*, vol. 268, 2022. <https://doi.org/10.1016/j.enbuild.2022.112155>
  20. Ma L., Huang Y., Zhao T. A synchronous prediction method for hourly energy consumption of abnormal monitoring branch based on the data-driven. *Energy and Buildings*, vol. 260, 2022. <https://doi.org/10.1016/j.enbuild.2022.111940>
  21. Nucci C.A., Borghetti A., Napolitano F., Tossani F. Basics of Power Systems Analysis. In: Papailiou K.O. (eds) *Springer Handbook of Power Systems*. Springer Handbooks. Springer, Singapore, 2021. [https://doi.org/10.1007/978-981-32-9938-2\\_5](https://doi.org/10.1007/978-981-32-9938-2_5)
  22. Sueta H.E., Santos S.R., Altafim R.A.C. Protection of Low-Voltage Equipment and Systems. In: Gomes C. (eds) *Lightning. Lecture Notes in Electrical Engineering*, vol 780. Springer, Singapore, 2021. [https://doi.org/10.1007/978-981-16-3440-6\\_5](https://doi.org/10.1007/978-981-16-3440-6_5)
  23. Li, J. (Ed.) *Overvoltage Mechanisms in Power Systems*. In *Measurement and Analysis of Overvoltages in Power Systems*, 2018. DOI: 10.1002/9781119129035
  24. Rudyk Y., Kuts V., Nazarovets O., Zdeb V. Complex Tools for Surge Process Analysis and Hardware Disturbance Protection. In: Ageyev D., Radivilova T., Kryvinska N. (eds) *Data-Centric Business and Applications. Lecture Notes on Data Engineering and Communications Technologies*, vol 69. Springer, Cham, 2021. [https://doi.org/10.1007/978-3-030-71892-3\\_9](https://doi.org/10.1007/978-3-030-71892-3_9)
  25. Alias W.N.H.A., Sujod M.Z., Kamari N.A.M. DC-Link Protection for Grid-Connected Photovoltaic System: A Review. In: Kasruddin Nasir A.N. et al. (eds) *ECCE2019. Lecture Notes in Electrical Engineering*, vol 632. Springer, Singapore, 2020. [https://doi.org/10.1007/978-981-15-2317-5\\_61](https://doi.org/10.1007/978-981-15-2317-5_61)
  26. Jin T., Yu Y., Elsayed E. Reliability and quality control for distributed wind/solar energy integration: a multi-criteria approach, *IIE Transactions*, 47:10, 1122-1138, 2015, DOI: [10.1080/0740817X.2015.1009199](https://doi.org/10.1080/0740817X.2015.1009199)
  27. Gupta N., Dogra R., Garg R., Kumar P. Review of islanding detection schemes for utility interactive solar photovoltaic systems, *International Journal of Green Energy*, 2021, DOI: [10.1080/15435075.2021.1941048](https://doi.org/10.1080/15435075.2021.1941048)
  28. Hashemi S., Østergaard J. Methods and strategies for overvoltage prevention in low voltage distribution systems with PV. *IET Renewable Power Generation*, 11: 205-214, 2017. <https://doi.org/10.1049/iet-rpg.2016.0277>

29. Pawar P., TarunKumar M., Vittal P.K. An IoT based Intelligent Smart Energy Management System with accurate forecasting and load strategy for renewable generation. *Measurement*, vol. 152, pp. 107187, 2020, <https://doi.org/10.1016/j.measurement.2019.107187>
30. Duer S. Assessment of the operation process of wind power plant's equipment with the use of an artificial neural network. *Energies*, 2020, 13, 2437, doi:10.3390/en13102437
31. Memon A.A., Laaksonen H., Kauhaniemi K. Microgrid Protection with Conventional and Adaptive Protection Schemes. In: Anvari-Moghaddam A., Abdi H., Mohammadi-Ivatloo B., Hatziargyriou N. (eds) *Microgrids. Power Systems*. Springer, Cham, 2021. [https://doi.org/10.1007/978-3-030-59750-4\\_19](https://doi.org/10.1007/978-3-030-59750-4_19)
32. Rock M. Protection of Selected Cases: PV Systems, Wind Turbines and Railway Systems. In: Gomes C. (eds) *Lightning. Lecture Notes in Electrical Engineering*, vol 780. Springer, Singapore, 2021. [https://doi.org/10.1007/978-981-16-3440-6\\_7](https://doi.org/10.1007/978-981-16-3440-6_7)
33. Azghandi, M.A., Barakati, S.M. A Temporary Overvoltages Mitigation Strategy for Grid-Connected Photovoltaic Systems Based on Current-Source Inverters. *Iran J Sci Technol Trans Electr Eng* 44, 1253–1262, 2020. <https://doi.org/10.1007/s40998-019-00291-7>
34. Sasi Kumar G., Radhika G., Ravi Kumar D. Reduction of Over Current and Over Voltage Under Fault Condition Using an Active SFCL with DG Units. In: Baredar P.V., Tangellapalli S., Solanki C.S. (eds) *Advances in Clean Energy Technologies*. Springer Proceedings in Energy. Springer, Singapor, 2021. [https://doi.org/10.1007/978-981-16-0235-1\\_54](https://doi.org/10.1007/978-981-16-0235-1_54)
35. Chetty L., Singh Y. Reliability Assessment of High Voltage Direct Current Grid Protection Schemes. *Quality and Reliability Engineering International*, 30, pages 1461–1472, 2014, <https://doi.org/10.1002/qre.1568>
36. El-kordy M., El-fergany A., Gawad A.F.A. Various Metaheuristic-Based Algorithms for Optimal Relay Coordination: Review and Prospective. *Arch Computat Methods Eng*, 28, 3621–3629, 2021. <https://doi.org/10.1007/s11831-020-09516-z>
37. Anisierowicz K. *Analysis of Electromagnetic Compatibility Problems in Extensive Objects under Lightning Threat*, Białystok University of Technology, Białystok 2005.
38. IEC 61662:1995. *Assessment of the Risk of Damage Due to Lightning*.
39. Bednarek M., Dąbrowski T., Olchowik W. Selected practical aspects of communication diagnosis in the industrial network. *J. KONBiN* 2019, 49, 383–404. DOI: 10.2478/jok-2019-0020. <https://doi.org/10.2478/jok-2019-0020>
40. Piersanti S., Orlandi A., Paulis de F. Electromagnetic absorbing materials design by optimization using a machine learning approach. *IEEE Transactions on Electromagnetic Compatibility*, pp. 1–8, 2018, DOI: 10.1109/TEM.2018.2871879.
41. Cao M.-Q., Liu T.-T., Zhu Y.-H., Shu J.-C., Cao M.-S. Developing electromagnetic functional materials for green building. *Journal of Building Engineering*, 45, 2022. <https://doi.org/10.1016/j.jobe.2021.103496>
42. Park G., Kim S., Park G.-K., Lee N. Influence of carbon fiber on the electromagnetic shielding effectiveness of high-performance fiber-reinforced cementitious composites. *Journal of Building Engineering*, 35, 2021. <https://doi.org/10.1016/j.jobe.2020.101982>
43. Skuza A., Ziemianek S., Suproniuk M. Power System Division—Certain Issues Associated with Shaping Commutation Strategies in Power Substations. *Energies*, 15, 9, 2022:7293. <https://doi.org/10.3390/en15197293>
44. Marchel P., Paska J., Pawlak K., Zagrajek K. A practical approach to optimal strategies of electricity contracting from Hybrid Power Sources. *Bulletin of the Polish Academy of Sciences, Technical Sciences*, 68, 1543–1551, 2020. <https://doi.org/10.24425/bpasts.2020.135377>
45. PN-EN 61000-4-5:2014. *Electromagnetic compatibility (EMC) - Part 4-5: Testing and measurement techniques - Surge immunity test*.
46. Borucka A. Maintaining technical readiness in the context of military exploitation systems. *Bulletin of the Polish Academy of Sciences, Technical Sciences*, 71, 5, 2023. <https://doi.org/10.24425/bpasts.2023.146619>
47. Kozłowski E., Borucka A., Oleszczuk P., Jałowicz T. Evaluation of the maintenance system readiness using the semi-Markov model taking into account hidden factors. *Eksplatacja i Niezawodność – Maintenance and Reliability*. 2023;25(4). <https://doi.org/10.17531/ein/172857>
48. Andrych-Zalewska M., Chlopek Z., Pielecha J., Merksiz J. Investigation of exhaust emissions from the gasoline engine of a light duty vehicle in the Real Driving Emissions test. *Eksplatacja i Niezawodność – Maintenance and Reliability*. 2023;25(2). <https://doi.org/10.17531/ein/165880>
49. Sawczuk W., Merksiz-Guranowska A., Rilo Cañas A., Kołodziejski S. New approach to brake pad wear modelling based on test stand friction-mechanical investigations. *Eksplatacja i Niezawodność – Maintenance and Reliability*. 2022;24(3):3. <https://doi.org/10.17531/ein.2022.3.3>

50. Yuan P., Pu Y., Liu C. Improving electricity supply reliability in China: Cost and incentive regulation. Energy, vol. 237, 2021. <https://doi.org/10.1016/j.energy.2021.121558>
51. Billinton R., Allan R. N. Reliability evaluation of power systems. New York: Plenum Press, 1996. <https://doi.org/10.1007/978-1-4899-1860-4>